IET Generation, Transmission & Distribution

Research Article

IET Journals
The Institution of Engineering and Technology

Multi-contingency TSCOPF based on full-system simulation

ISSN 1751-8687
Received on 10th March 2016
Revised on 1st August 2016
Accepted on 24th August 2016
doi: 10.1049/iet-gtd.2016.0355
www.ietdl.org

Pablo Ledesma[1] ✉, *Ignacio Antonio Calle*[2], *Edgardo Daniel Castronuovo*[1], *Francisco Arredondo*[1]

[1]*Electrical Engineering Department, Universidad Carlos III de Madrid, Av. Universidad 30, 28911 Leganés, Spain*
[2]*Electrical Engineering Department, Universidad Técnica Federico Santa María, Av. España 1680, Valparaíso, Chile*
✉ *E-mail: pablole@ing.uc3m.es*

Abstract: Transient stability constrained optimal power flow (TSCOPF) is a non-linear optimisation problem used to perform economic dispatches while ensuring TS. This study proposes a multi-contingency TSCOPF model that retains the dynamics of all generators and includes a transient synchronous generator fourth-order *dq*-axis model. A program is developed that automatically reads the system data from standard files, builds the multiple-contingency TSCOPF model on a high-level modelling system and solves it using a non-heuristic interior point algorithm. This approach facilitates the application of the model to a variety of systems and scenarios. A TSC based on the speed deviation instead of the rotor angle is proposed. Results obtained on several standard systems are shown. The proposed method is applied to the northwest Spanish transmission system to obtain an optimised dispatch that ensures TS after any of a number of faults, and to assess the economic impact of fault-clearing times at different substations.

Nomenclature

Name	Variable	Units
E'^t_d, E'^t_q	generator internal transient voltage components	pu
E^t_{fd}, $E^t_{fdexc,i}$	field voltage and field voltage signal	pu
I^t_d, I^t_q	generator output current components	pu
I_G	magnitude of generator output current	pu
I_{mn}	current between buses m and n	pu
P^t_e	generator active power output	pu
P_G, Q_G	pre-fault generator active and reactive power outputs	pu
V	bus voltage magnitude	pu
V^t_{term}	voltage at the generator connection bus	pu
α	bus voltage phase	rad
δ^t	rotor angle	rad
ΔP^t	turbine governor output	pu
$\Delta\omega^t_{COI}$	centre of inertia speed deviation	pu
$\Delta\omega^t$	generator speed deviation	pu
φ	bus angle between current and voltage	rad
D	damping coefficient	pu
H	inertia constant	s
$()^{MAX}$ $()^{MIN}$	upper and lower limits of the variables	
K_{EXC}	excitation system gain	pu
K_{TG}	turbine governor gain	pu
r_a	armature resistance	pu
P_D, Q_D	active and reactive power demands	pu
T'_{d0}, T'_{q0}	generator transient time constants	S
T_{EXC}	excitation system time constant	S
T_{TG}	turbine governor time constant	s
V_{ref}	excitation system voltage reference	pu
x_d, x_q	*dq*-axis synchronous reactances	pu
$\boldsymbol{Y}$	reduced admittance matrix	pu
$\boldsymbol{Y}^{bus}$	bus admittance matrix	pu
Y_{ij}	magnitude of the element (i,j) of $\boldsymbol{Y}$	pu
Y^{bus}_{mn}	magnitude of the element (m,n) of $\boldsymbol{Y}^{bus}$	pu
Δt	time step	s
θ_{ij}	phase of the element (i,j) of $\boldsymbol{Y}$	rad
θ^{bus}_{mn}	phase of the element (m,n) of $\boldsymbol{Y}^{bus}$	rad
ω_0	frequency reference	rad/s

Sets

$\mathcal{G}$	generators
$\mathcal{L}$	non-generator buses
$\mathcal{N}$	buses
$\mathcal{T}$	time steps

1 Introduction

Transient stability constrained optimal power flow (TSCOPF) is an optimisation problem that simultaneously includes static and dynamic constraints in the formulation. TSCOPF has received growing interest in the last decade as a tool for preventing transient instability because of its combination of economic objectives, steady-state PF equations and dynamic simulations in a single model [1–3].

To be a useful tool in dynamic security assessment, a TSCOPF model must represent the dynamics of the network with sufficient accuracy, comparable with that of the dynamic simulations routinely performed by transmission system operators. The high non-linearity of electromechanical oscillations in power systems makes TSCOPF models difficult to solve. As the corresponding programming model has a very large dimension and requires heavy computation, most of the effort in this field have been centred on reducing the scale of the problem and improving computation efficiency. Some studies apply iterative algorithms, running the dynamic simulation of a fault and correcting the generation dispatch at each iteration [4–8]. In some cases, time-domain simulations are run on commercial software such as power system simulator for engineering (PSSE) [9, 10]. This approach makes it possible to increase the detail and complexity of the dynamic model, but poses the problem of dealing with unstable cases that may result in numerical failure of the time-domain simulator. Other studies make use of direct methods to reduce the size and complexity of the optimisation model [11–16], relying on reduced dynamic models such as the single-machine equivalent. These works apply several iterations to refine the heuristic constraints, are usually applied to single fault studies with few exceptions [17] and can be used on power systems of virtually any size, but rely on a simplified model and can be ill-suited for complex patterns of oscillations [1]. In [18], a transformation of the original formulation to the Euclidean space is applied to analyse the stability of the system without representing the trajectories of the variables, but this approach makes it difficult to evaluate the behaviour of the variables after the fault. Similar approaches are followed in [19, 20], where Lyapunov functions are used, and [21].

Multi-contingency (MC) studies and complex multi-machine oscillations can be addressed if fault and post-fault states of different contingencies are included in the optimisation model and the dynamics of all synchronous machines are preserved. This paper applies an MC TSCOPF model that preserves the dynamics of all synchronous machines during the analysed time frame, and that includes a transient fourth-order *dq*-axis dynamic model of the synchronous generator that represents electromagnetic transients in the rotor. The model is intended for systems in the size of tens of generators or reduced areas within larger power systems. The differential equations corresponding to the fault and post-fault dynamics of different contingencies are discretised using the trapezoidal rule and included as algebraic equations. The main drawbacks of this approach are the size and complexity of the resulting model. Previous works that use this technique are usually applied to small systems [22–24] and use the classical synchronous generator model, though this model is generally regarded as inaccurate for TS studies [25]. Significant advances in terms of computational time have been achieved using dedicated solvers [26] and parallel computing [27], though these works are also limited to the classical generator model. An interesting approach has recently combined a sequential and a simultaneous method [28] that makes it possible to increase the size and the detail of the model. Recently, the application field of transient constrained dispatch has also been expanded to the unit commitment problem [29, 30].

This paper presents a software framework that facilitates the application of the proposed MC TSCOPF model. It includes a program developed in Python language that reads the data of a transmission system in standard PSSE format and automatically constructs the model in general algebraic modelling system (GAMS) language [31]. The model is then compiled and solved using a standard non-linear programming (NLP) solver. No time-domain simulations are required outside the GAMS solver. The result is a flexible and efficient tool in which the modelling of multiple contingencies is straightforward and the trajectories of the variables can be analysed directly on the solution.

The main contributions of this paper are:

- A software framework to apply MC TSCOPF analysis to power systems. Input data are taken from PSSE standard files and the whole process is made transparent to the user. The model is constructed in a high-level modelling system, which facilitates the use of off-the-self solvers.
- The inclusion of a fourth-order transient synchronous generator model in the proposed MC TSCOPF model.
- The implementation of a TS constraint based on rotor speed deviation, which is better suited for large systems than the rotor angle constraints commonly used in TSCOPF.

The proposed tool is used to calculate the optimal dispatch that ensures TS, the increase in cost with respect to the OPF and the economic impact of fault-clearing times (FCTs). Results are shown on several standard test cases and on the northwest Spanish Peninsular System.

This paper is organised as follows: Section 2 shows the TSCOPF mathematical model; Section 3 explains the practical framework used to apply the model; Section 4 discusses the TS criterion based on the speed deviation; Section 5 shows results obtained on several test cases and on the Spanish northwest power system; and Section 6 is the conclusion.

2 Mathematical model

TS analysis involves three periods: pre-fault, fault and post-fault. These periods are explicitly included in the TSCOPF model as equality and inequality constraints. The pre-fault stage, as in any conventional OPF, is represented by equality constraints that correspond to PF equations [32] and inequality constraints that represent limits on the production of power plants, on the voltage at buses and on the current through lines and transformers [33]. The initialisation of dynamic variables also corresponds to the pre-fault stage. During the fault and post-fault periods, loads are represented as constant admittances. The Kron reduction is applied to the admittance matrix to retain only the internal nodes of the generators and reduce the computational effort, a usual procedure in TSCOPF.

The complete set of equations of the optimisation model is

$$\min f(P_{\mathrm{G}i}) = \sum_{\forall i} \left(a_i P_{\mathrm{G}i}^2 + b_i P_{\mathrm{G}i} + c_i\right) \tag{1}$$

subject to

$$\left.\begin{aligned} P_{\mathrm{G}i} - P_{\mathrm{D}i} - V_i \sum_{\forall n} V_n Y_{\mathrm{in}}^{\mathrm{Bus}} \cos\left(\alpha_i - \alpha_n - \theta_{\mathrm{in}}^{\mathrm{Bus}}\right) = 0 \\ Q_{\mathrm{G}i} - Q_{\mathrm{D}i} - V_i \sum_{\forall n} V_n Y_{\mathrm{in}}^{\mathrm{Bus}} \sin\left(\alpha_i - \alpha_n - \theta_{\mathrm{in}}^{\mathrm{Bus}}\right) = 0 \end{aligned}\right\} \tag{2}$$

$$\left.\begin{aligned} P_{\mathrm{D}l} + V_l \sum_{\forall n} V_n Y_{\mathrm{ln}}^{\mathrm{Bus}} \cos\left(\alpha_l - \alpha_n - \theta_{\mathrm{ln}}^{\mathrm{Bus}}\right) = 0 \\ Q_{\mathrm{D}l} + V_l \sum_{\forall n} V_n Y_{\mathrm{ln}}^{\mathrm{Bus}} \sin\left(\alpha_l - \alpha_n - \theta_{\mathrm{ln}}^{\mathrm{Bus}}\right) = 0 \end{aligned}\right\} \tag{3}$$

(see (4))

$$\left(I_{\mathrm{G}i} V_i\right)^2 - P_{\mathrm{G}i}^2 - Q_{\mathrm{G}i}^2 = 0 \tag{5}$$

$$\sin\,\varphi_i - Q_{\mathrm{G}i}/V_i I_{\mathrm{G}i} = 0 \tag{6}$$

$$\left.\begin{aligned} E'^0_{di} - \left(x_{qi} - x'_{qi}\right) I_{\mathrm{G}i} \cos\left(\delta_i^0 - \alpha_i + \varphi_i\right) = 0 \\ E'^0_{qi} + \left(x_{di} - x'_{di}\right) I_{\mathrm{G}i} \sin\left(\delta_i^0 - \alpha_i + \varphi_i\right) - E^0_{\mathrm{f}di} = 0 \end{aligned}\right\} \tag{7}$$

(see (8))

$$\left.\begin{aligned} I_{di}^0 - I_{\mathrm{G}i} \sin\left(\delta_i^0 - \alpha_i + \varphi_i\right) = 0 \\ I_{qi}^0 - I_{\mathrm{G}i} \cos\left(\delta_i^0 - \alpha_i + \varphi_i\right) = 0 \end{aligned}\right\} \tag{9}$$

(see (10))

(see equations (11)–(13) at the bottom of the next page)

$$\delta_i^{t+1} - \delta_i^t - \frac{\Delta t}{2}\omega_0\left(\Delta\omega_i^{t+1} + \Delta\omega_i^t\right) = 0 \tag{14}$$

(see equations (15) and (16) at the bottom of the next page)

$$I_{mn}^2 - Y_{mn}^{\mathrm{Bus}\,2}\left[\left(V_m \cos\,\alpha_m - V_n \cos\,\alpha_n\right)^2 + \left(V_m \sin\,\alpha_m - V_n \sin\,\alpha_n\right)^2\right] = 0 \tag{4}$$

$$\left.\begin{aligned} V_i \sin\left(\delta_i^0 - \alpha_i\right) - E'^0_{di} + I_{\mathrm{G}i}\left[r_{ai} \sin\left(\delta_i^0 - \alpha_i + \varphi_i\right) - x'_{qi} \cos\left(\delta_i^0 - \alpha_i + \varphi_i\right)\right] = 0 \\ V_i \cos\left(\delta_i^0 - \alpha_i\right) - E'^0_{qi} + I_{\mathrm{G}i}\left[r_{ai} \cos\left(\delta_i^0 - \alpha_i + \varphi_i\right) + x'_{di} \sin\left(\delta_i^0 - \alpha_i + \varphi_i\right)\right] = 0 \end{aligned}\right\} \tag{8}$$

$$K_{\mathrm{EXC}i}\left(V_{\mathrm{ref}i} - V^0_{\mathrm{term}i}\right) - E^0_{\mathrm{f}d\mathrm{exc},\,i} = 0; \quad \Delta P_i^0 = 0;\ P_{ei}^0 - P_{\mathrm{G}i} = 0; \quad \Delta\omega_i^0 = 0 \tag{10}$$

$$P_{ei}^{t} - E'^{t}_{di} I_{di}^{t} - E'^{t}_{qi} I_{qi}^{t} = 0 \tag{17}$$

$$\left.\begin{aligned} I_{di}^{t} - \sum_{\forall j} Y_{ij}\left(E'^{t}_{d_j} \cos\left(\delta_i^t - \delta_j^t - \theta_{ij}\right) + E'^{t}_{qj} \sin\left(\delta_i^t - \delta_j^t - \theta_{ij}\right)\right) = 0 \\ I_{qi}^{t} - \sum_{\forall j} Y_{ij}\left(E'^{t}_{q_j} \cos\left(\delta_i^t - \delta_j^t - \theta_{ij}\right) - E'^{t}_{dj} \sin\left(\delta_i^t - \delta_j^t - \theta_{ij}\right)\right) = 0 \end{aligned}\right\} \tag{18}$$

$$V_{\text{term},i}^{t2} - \left(E'^{t}_{di} + x'_{di} I_{qi}^{t}\right)^2 + \left(E'^{t}_{qi} - x'_{di} I_{di}^{t}\right)^2 = 0 \tag{19}$$

$$\Delta\omega_{\text{COI}}^{t} - \sum_{\forall i} H_i \Delta\omega_i^t / \sum_{\forall i} H_i = 0 \tag{20}$$

$$0 \le P_{\text{G}i} \le P^{\text{MAX}}; \quad 0 \le I_{\text{G}i} \le I_{\text{G}i}^{\text{MAX}} \tag{21}$$

$$V^{\text{MIN}} \le V_m \le V^{\text{MAX}}; \quad -I_{mn}^{\text{MAX}} \le I_{mn} \le I_{mn}^{\text{MAX}}; \quad E_{\text{f}d}^{\text{MIN}} \le E_{\text{f}di}^{0} \le E_{\text{f}d}^{\text{MAX}} \tag{22}$$

$$-\Delta\omega^{\text{MAX}} \le \Delta\omega_i^t - \Delta\omega_{\text{COI}}^t \le \Delta\omega^{\text{MAX}} \tag{23}$$

$$\forall i, j \in \{\mathcal{G}\}; \quad \forall l \in \{\mathcal{L}\}; \quad \forall m, n \in \{\mathcal{N}\}; \quad \forall t \in \{\mathcal{T}\}$$

The objective function (1) is the power generation cost, calculated as a quadratic function. However, other conventional cost functions can be used to minimise deviation with respect to a schedule, to minimise power losses etc.

Equations (2)–(10) correspond to the pre-fault stage. Equality constraints (2) and (3) represent the balance between input and output powers in the generation and non-generation buses. Equation (4) calculates the current through the branches (lines and transformers). Equations (5) and (6) calculate the output current and power factor of the generators. Equations (7)–(10) calculate the initial conditions of the state variables.

Equations (11)–(14) result from the application of the trapezoidal rule to the differential equations of the transient synchronous fourth-order generator model [34, 35]

$$\frac{\text{d}E'_{di}}{\text{d}t} = \frac{1}{T'_{q0i}}\left(-E'_{di} + \left(x_{qi} - x'_{qi}\right) I_{qi}\right) \tag{24}$$

$$\frac{\text{d}E'_{qi}}{\text{d}t} = \frac{1}{T'_{d0i}}\left(-E'_{qi} - \left(x_{di} - x'_{di}\right) I_{di} + E_{\text{f}di}\right) \tag{25}$$

$$\frac{\text{d}\Delta\omega_i}{\text{d}t} = \frac{1}{2H_i}\left(P_{mi} - P_{ei} - D_i \Delta\omega_i\right) \tag{26}$$

$$\frac{\text{d}\delta_i}{\text{d}t} = \omega_0 \Delta\omega_i \tag{27}$$

The interface between the synchronous generator and the grid consists of a voltage source $E'_{di} + \text{j}E'_{qi}$ behind an impedance $r_{ai} + \text{j}x'_{di}$. Machine variables are referred to a dq reference frame fixed to the rotor, while grid variables are usually referred to a common synchronous rotating $\alpha\beta$ reference frame. Fig. 1 shows both reference frames, together with internal voltage E'_i and output current I_i. The rotation equations needed to change from one machine reference frame to other are implicitly included in the model. This removes all $\alpha\beta$–dq rotations and reduces the number of equality constraints in the optimisation model.

Equation (15) results from the application of the trapezoidal rule to the turbine governor model

$$\frac{\text{d}\Delta P_i}{\text{d}t} = -\frac{1}{T_{\text{TG}i}}\left(K_{\text{TG}i}\Delta\omega_i + \Delta P_i\right) \tag{28}$$

Equation (16) results from the application of the trapezoidal rule to the voltage regulator model, which is a reduced version of the simplified excitation system [36] and includes a limit on the field voltage

$$\left.\begin{aligned} \frac{\text{d}E_{\text{f}d\text{exc},i}}{dt} &= \frac{1}{T_{\text{EXC}i}}\left[-E_{\text{f}d\text{exc},i} + K_{\text{EXC}i}\left(V_{\text{ref}i} - V_{\text{term},i}\right)\right] \\ E_{\text{f}di} &= \min\left\{E_{\text{f}d\text{exc},i},\ E_{\text{f}di\text{MAX}}\right\} \\ E_{\text{f}di} &= \max\left\{E_{\text{f}d\text{exc},i},\ E_{\text{f}di\text{MIN}}\right\} \end{aligned}\right\} \tag{29}$$

Equation (17) calculates the active power output of the generators at each time step. Equation (18) calculates the current in the generators as a function of the reduced admittance matrix $\boldsymbol{Y}$. Equation (19) calculates terminal voltage V_{term}. Equation (20) calculates the centre of inertia (COI) speed deviation, which is later used in the TS constraint. Equations (21) represent the capability limits of the generators. Equation (22) defines limits to bus voltages, branch currents and machine initial field voltages. The rest of the variables are also maintained within specified large limits, as it is usually done in constrained optimisation.

$$E'^{t+1}_{di}\left(1 + \frac{\Delta t}{2}\frac{1}{T'_{q0i}}\right) - E'^{t}_{di}\left(1 - \frac{\Delta t}{2}\frac{1}{T'_{q0i}}\right) - \frac{\Delta t}{2}\frac{1}{T'_{q0i}}\left(x_{qi} - x'_{qi}\right)\left(I_{qi}^{t+1} + I_{qi}^{t}\right) = 0 \tag{11}$$

$$E'^{t+1}_{qi}\left(1 + \frac{\Delta t}{2}\frac{1}{T'_{d0i}}\right) - E'_{qi}t\left(1 - \frac{\Delta t}{2}\frac{1}{T'_{d0i}}\right) - \frac{\Delta t}{2}\frac{1}{T'_{d0i}}\left[\left(E_{fdi}^{t+1} + E_{fdi}^{t}\right) - \left(x_{di} - x'_{di}\right)\left(I_{di}^{t+1} + I_{di}^{t}\right)\right] = 0 \tag{12}$$

$$\Delta\omega_i^{t+1}\left(1 + D_i\frac{\Delta t}{2}\frac{1}{2H_i}\right) - \Delta\omega_i^{t}\left(1 - D_i\frac{\Delta t}{2}\frac{1}{2H_i}\right) - \frac{\Delta t}{2}\frac{1}{2H_i}\left(2P_{mi} + \Delta P_i^{t+1} + \Delta P_i^{t} - P_{ei}^{t+1} - P_{ei}^{t}\right) = 0 \tag{13}$$

$$\Delta P_i^{t+1}\left(1 + \frac{\Delta t}{2}\frac{1}{T_{\text{TG}i}}\right) - \Delta P_i^{t}\left(1 - \frac{\Delta t}{2}\frac{1}{T_{\text{TG}i}}\right) + \frac{\Delta t}{2}\frac{K_{\text{TG}i}}{T_{\text{TG}i}}\left(\Delta\omega_i^{t+1} + \Delta\omega_i^{t}\right) = 0 \tag{15}$$

$$\left.\begin{aligned} E_{\text{f}d\text{exc},i}^{t+1}\left(1 + \frac{\Delta t}{2}\frac{1}{T_{\text{EXC}i}}\right) - E_{\text{f}d\text{exc},i}^{t}\left(1 - \frac{\Delta t}{2}\frac{1}{T_{\text{EXC}i}}\right) - \frac{\Delta t}{2}\frac{K_{\text{EXC}i}}{T_{\text{EXC}i}}\left(2V_{\text{ref}i} - V_{\text{term},i}^{t+1} - V_{\text{term},i}^{t}\right) = 0 \\ E_{\text{f}di}^{t} = \min\left\{E_{\text{f}d\text{exc},i}^{t},\ E_{\text{f}di\text{MAX}}\right\} \\ E_{\text{f}di}^{t} = \max\left\{E_{\text{f}d\text{exc},i}^{t},\ E_{\text{f}di\text{MIN}}\right\} \end{aligned}\right\} \tag{16}$$

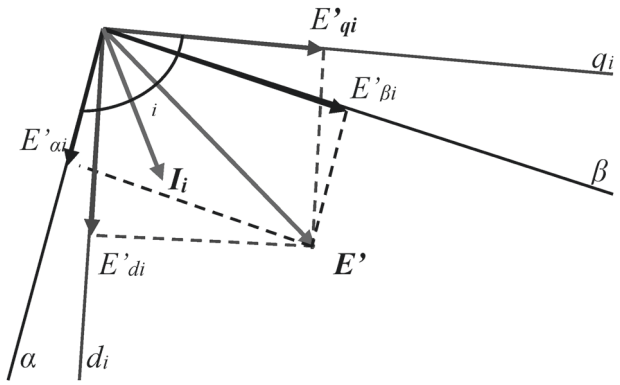

Fig. 1 *Internal voltage, output current and reference frames for the ith generator*

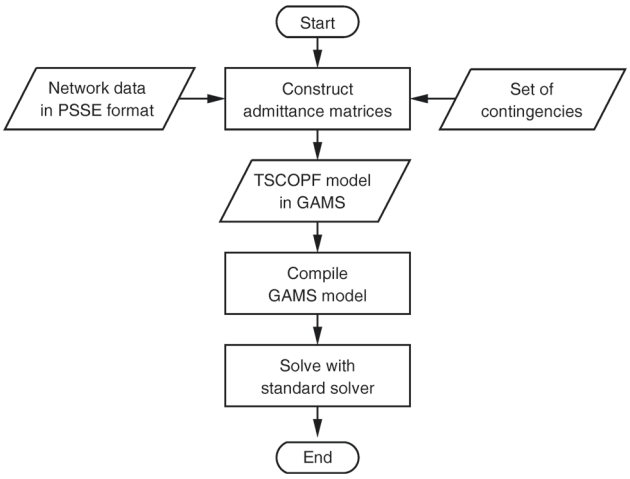

Fig. 2 *Flowchart showing the building and solution of the MC TSCOPF model*

Equation (23) is the TS constraint, which is based on the synchronous machines speed deviation as explained in Section 4.

MC analysis is provided by replicating variables $\left\{E'_{di},\ E'_{qi},\ I_{di},\ I_{qi},\ \delta_i,\ \Delta\omega_i,\ \Delta\omega_{\mathrm{COI}},\ \Delta P_i,\ P_{ei},\ E_{\mathrm{f}di},\ E_{\mathrm{f}\mathrm{dexc},i}\right\}$ and (11)–(20) for each contingency in the optimisation model. As steady-state variables are unique in the optimisation model, the optimal solution guarantees that all generators will maintain synchronism if any of the modelled contingencies occurs.

3 Practical application framework

One of the advantages of the adopted approach is that the model is directly handled by a generic NLP solver. No previous discrimination between critical and non-critical machines is needed. However, the size and complexity of the optimisation model formulated in Section 2 make it laborious to build the equations even for small systems. Furthermore, subsequent changes in the system to represent different operation points or different set of faults require to rewrite large parts of the model. To make the model useful from a practical point of view, the automatic procedure depicted in Fig. 2 is implemented.

The power system topology, the PF data, the dynamic parameters and the static constraints are read from standard files. In this case, PSSE raw files are used because PSSE is the program used by the Spanish transmission system operator to simulate the transmission system. Information about the location of the faults and the switching operations applied to clear them is written in another file. A Python program reads these files, constructs the pre-fault, fault and post-fault admittance matrices, and writes the complete model in GAMS language. The model is then fed into a GAMS interpreter, compiled and solved using a generic NLP solver. The results provided in this paper are obtained using interior point optimiser (IPOPT) an open source software package for large-scale non-linear optimisation that implements an interior point line search filter method [37, 38].

The Python program is central to this scheme. It builds the TSCOPF GAMS model, making the most laborious part of the procedure transparent to the user. Fig. 3 shows the correlations between the input data and the equations of the optimisation model described in Section 2. The source code corresponding to the Python program and the GAMS file has been made publicly available from a public server as explained in the Appendix.

Changes in the network topology, the load or the power system constraints can be applied using the PSSE graphical user interface before running the MC TSCOPF. The result is a flexible tool that facilitates the application to different systems, scenarios, sets of faults and solvers.

4 TS criterion

Previous works on TSCOPF implement the TS constraint as a limit on the rotor angles, typically 100° with respect to the COI angle [22–25]. This constraint is well suited for small power systems,

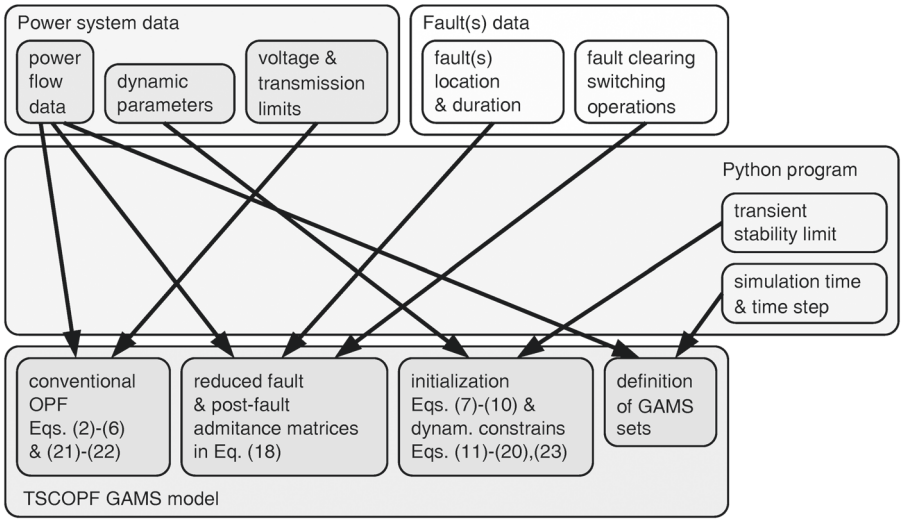

Fig. 3 *Automatic building of the TSCOPF GAMS model*

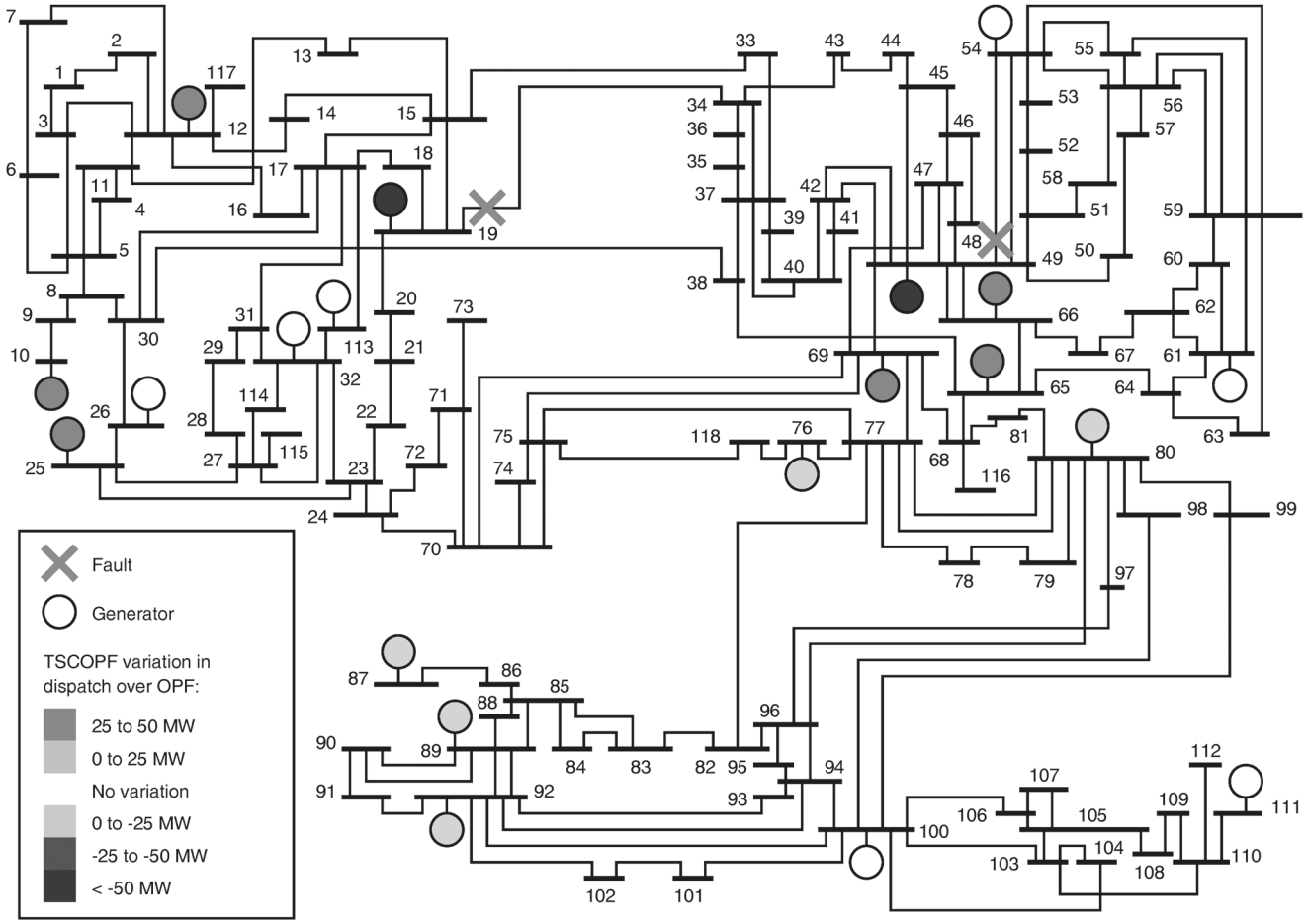

Fig. 4 *IEEE 118 bus test system. The fault locations and changes in dispatch correspond to the study as shown in Section 5.1*

but can result in conservative solutions when applied to relatively large systems, because large voltage angle differences can exist between parts of the system as a result of pre-fault PFs and not as a result of any instability. For example, [42, Fig. D1a] shows a case taken from the continental Europe power system in which voltage phase angle differences between the North and the South of Europe are larger than 110°.

In this paper, the TS constraint is defined as a limit on the rotor speed deviation of every generator with respect to the COI speed deviation. This ensures that the stability constraint is violated only if one or more machines lose synchronism with respect to the rest of the system, regardless of the angle differences in the steady-state operating point.

The advantage of the rotor angle over the speed deviation as a TS criterion is illustrated by a case taken from the IEEE 118 bus system, depicted in Fig. 4. The pre-fault rotor angles of the 20 synchronous generators are shown in Table 1. Fig. 5 shows the speed deviations (a) and rotor angles (b) after a fault at bus 13. It can be seen that the case is stable and that all speed deviations remain within the stability limit. However, rotor angles violate the angular stability limit $\delta_{\mathrm{COI}} \pm 100°$. In this case, the rotor angle stability criterion would lead to a conservative solution. While the rotor angle limit can be expanded to account for pre-fault large angle differences, this would risk accepting unstable cases or require larger simulation times with the consequent increase in model size.

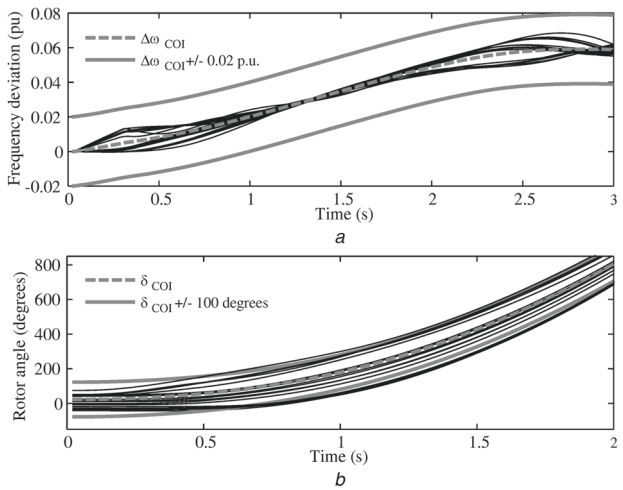

Fig. 5 *Speed and angle stability criteria in an IEEE 118 bus system stable case*

a Synchronous generator frequency deviation
b Synchronous generator rotor angle

Table 1 IEEE 118 bus system initial operating point

Generator	10	12	19	25	26	32	49	54	61	65	66	69	76	80	87	89	92	100	111	113
δ_o, deg	74	50	48	47	47	49	43	41	50	16	24	−1	10	−7	−18	−35	−26	−31	−42	40

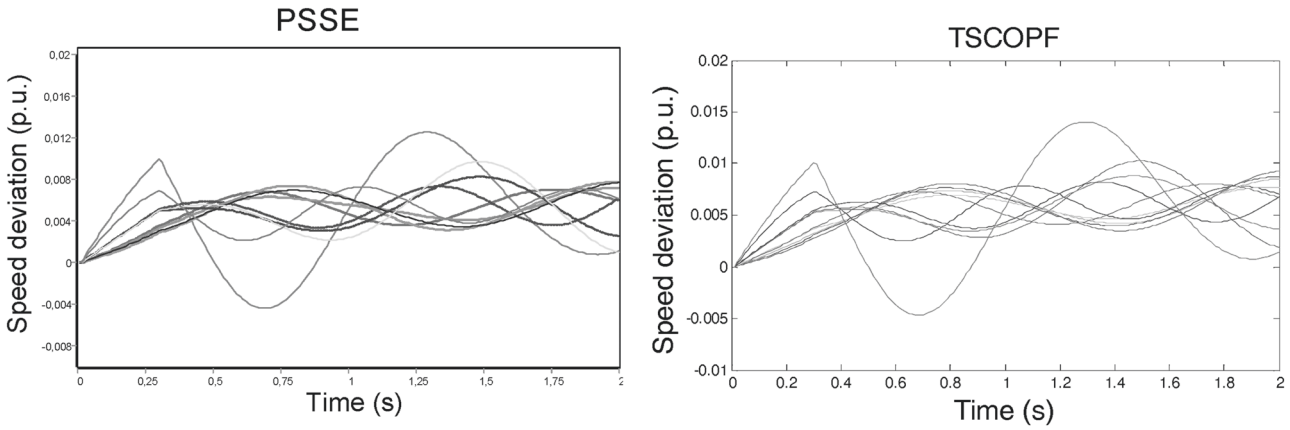

Fig. 6 *Comparison between the solution of the TSCOPF model and a time-domain simulation in PSSE*

Table 2 Solution of the TSCOPF including one fault

	Six bus	IEEE 30	IEEE 57	New England	IEEE 118
size ($\mathcal{N}/\mathcal{G}$)	6/3	30/6	57/7	39/10	118/20
number of variables	3189	5119	6004	8454	21,049
Number of constraints	3889	6193	7257	10,243	25,498
number of iterations	27	23	44	59	43
memory usage, MB	4.2	3.9	15.9	60.4	68.2
CPU time, s					
compilation	<0.1	<0.1	<0.1	<0.1	<0.1
model generation	0.184	0.203	0.257	0.412	1.13
NLP functions evaluation	0.43	0.57	1.8	10.8	56
solver IPOPT	5	3	10	60	375

Table 3 Solution of the TSCOPF including two faults

	Six bus	IEEE 30	IEEE 57	New England	IEEE 118
size ($\mathcal{N}/\mathcal{G}$)	6/3	30/6	57/7	39/10	118/20
number of variables	6414	10,146	11,854	16,777	41,752
number of constraints	7747	12,286	14,351	20,341	50,624
number of iterations	74	30	75	65	49
memory usage, MB	4.9	11.1	19.2	107	258.3
CPU time, s					
compilation	<0.1	<0.1	<0.1	<0.1	<0.1
model generation	0.224	0.264	0.341	0.628	1.92
NLP functions evaluation	0.95	0.97	3.0	16.4	84
solver IPOPT	8	10	34	135	535

5 Results

5.1 Application to standard test systems

The proposed method is first applied to several standard cases to show its performance and to evaluate the computational cost of the solution. The following systems are studied: six bus system described in [35], IEEE 30 bus, IEEE 57 bus, New England 39 bus and IEEE 118 buses test cases [39–41].

The solution of the TSCOPF model has been checked against a time-domain simulation in PSSE. Fig. 6 shows the speed deviation of the synchronous generators in the New England 39 bus system when a fault is applied at bus 31. Time step Δt is 0.01 s in both the TSCOPF model and the PSSE simulation.

The performance of the algorithm when applied to one and two faults is shown in Tables 2 and 3, respectively. The central processing unit (CPU) times correspond to the solution using GAMS and solver IPOPT on a computer with a 2.5 GHz processor and a Linux operating system. In all cases, no convergence problems are observed.

It can be seen that the main factor affecting CPU time is the number of generators. The New England power system, for example, has more generators, but fewer buses than the IEEE 57 bus system, and the resulting CPU time is longer. The reason is that the size of the reduced admittance matrix $\boldsymbol{Y}$ is proportional to the square of the number of generators.

The size of the optimisation model increases almost linearly with the number of contingencies analysed. The CPU time, however, does not increase always linearly because the solution of some faults is computationally more demanding than others.

A deeper analysis of the solutions is performed in the IEEE 118 buses, the largest showed in this section, depicted in Fig. 4. Two different three-phase short-circuits are analysed on the system: one at bus 19, cleared by the disconnection of line 19–34 after 300 ms;

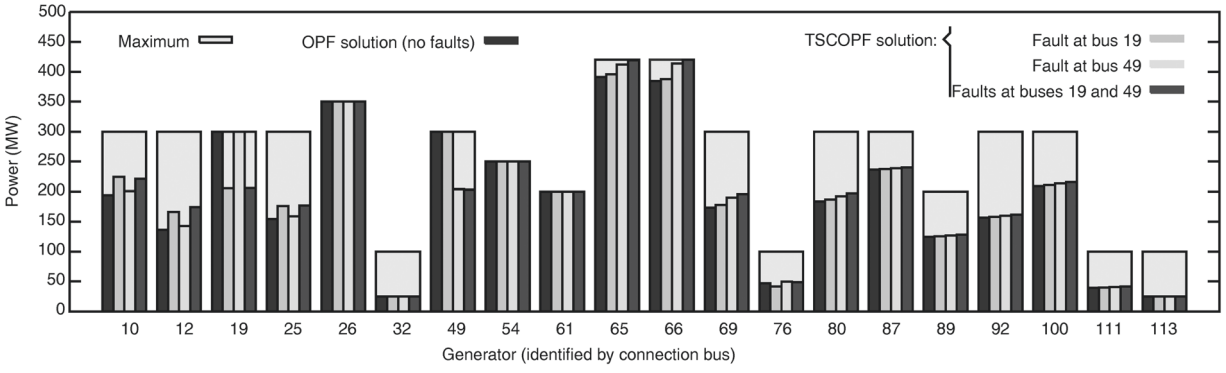

Fig. 7 *Effect of the TSCOPF on the dispatch of the IEEE 118 bus system*

Table 4 Comparison between TS limits

Stability criterion	ΔCost with respect to OPF, M.U.
$\omega_i - \omega_{COI} < 0.005$ pu	unfeasible
$\omega_i - \omega_{COI} < 0.01$ pu	3112
$\omega_i - \omega_{COI} < 0.013$ pu	2382
$\omega_i - \omega_{COI} < 0.015$ pu	1295
$\omega_i - \omega_{COI} < 0.02$ pu	1295
$\omega_i - \omega_{COI} < 0.04$ pu	1295
$\delta_i - \delta_{COI} < 50°$	1369
$\delta_i - \delta_{COI} < 100°$	1295

the other one at bus 49, cleared by the disconnection of line 49–54 after 300 ms. Buses 19 and 49 are selected because they are critical from the point of view of TS: first, they are central buses with a relatively large number of incoming lines, and second they are connected to generators that are more likely to lose synchronism because they are dispatched at full load by the OPF. For more information about the IEEE 118 bus system and the coefficients in the cost function, see the Appendix.

Fig. 7 shows the production of the different generators according to (i) the conventional OPF resulting from solving an optimisation problem only with (2)–(6) and (21)–(22), (ii) the TSCOPF considering the fault at bus 19, (iii) the TSCOPF considering the fault at bus 49 and (iv) an MC-TSCOPF including both faults. It can be seen that the main effect of the TSCOPF is the reduction of the production of the generators connected at the faulted buses. As these generators cannot maintain stability after the fault when operating at full load, the solution of the TSCOPF reduces their production to comply with the stability constraints. When faults at buses 19 and 49 are studied separately, the optimal solution of the TSCOPF results in a cost increase of 450.0 M.U. (Monetary Units) and 773.8 M.U. with respect to a conventional OPF. When both faults are simultaneously included in the MC model, the solution of the MC TSCOPF results in a cost increase of 1294.7 M.U. The effect of the MC TSCOPF can be also observed in Fig. 4, in which the colours of the generators represent the variation in the dispatch provided by the MC TSCOPF with respect to the dispatch of the OPF.

Several speed deviation limits have been simulated to select the value used in the study. Table 4 shows the cost obtained with each limit. A limit too low results in TSCOPFs too conservative ($|\omega_i - \omega_{COI}| < 0.01$, 0.013 pu) or even unfeasible ($|\omega_i - \omega_{COI}| < 0.005$ pu). A maximum deviation of 0.02 pu has been found experimentally to be a good value to discriminate between stable and unstable cases. The costs for two maximum angle limits are also shown for comparison; in this particular case, a maximum angle $|\delta_i - \delta_{COI}| < 100°$ serves also as a good TS constraint, because there are no large voltage angle differences in the steady-state solution.

Fig. 8 shows the speed deviations and active power productions provided by the optimal solution of the two-faults MC TSCOPF. The speeds of the generators are constrained within a band of 0.02 pu above and below the speed of the COI. It can be seen that after either of the faults, the speed deviation is maintained inside the specified limits. The generator closest to the fault is the most affected by the fault in terms of speed deviation and active power oscillations.

An interesting application of the proposed model is as a tool to assess the selection of short-circuit protection devices. Faster protections can improve TS, but it is difficult to evaluate their economic impact without using an MC TSCOPF. A systematic study of the effect of the protection speed has been performed, solving the MC TSCOPF model with different FCTs from 200 to 300 ms. Results are shown in Fig. 9. It can be seen that a reduction of the operating cost from 1294 to 536 M.U. (59%) can be achieved if the FCT is reduced from 300 to 220 ms for both faults. It can also be seen that the savings obtained by the reduction of the FCT at bus 49 is 54% larger than the savings obtained by the reduction at bus 19.

5.2 Application to the Spanish northwest power system

The Spanish northwest power system is a meshed transmission grid connected to the Spanish and Portuguese systems through two substations (Castelle and La Lomba). Fig. 10 shows all 380 kV lines, together with the main power plants in the area.

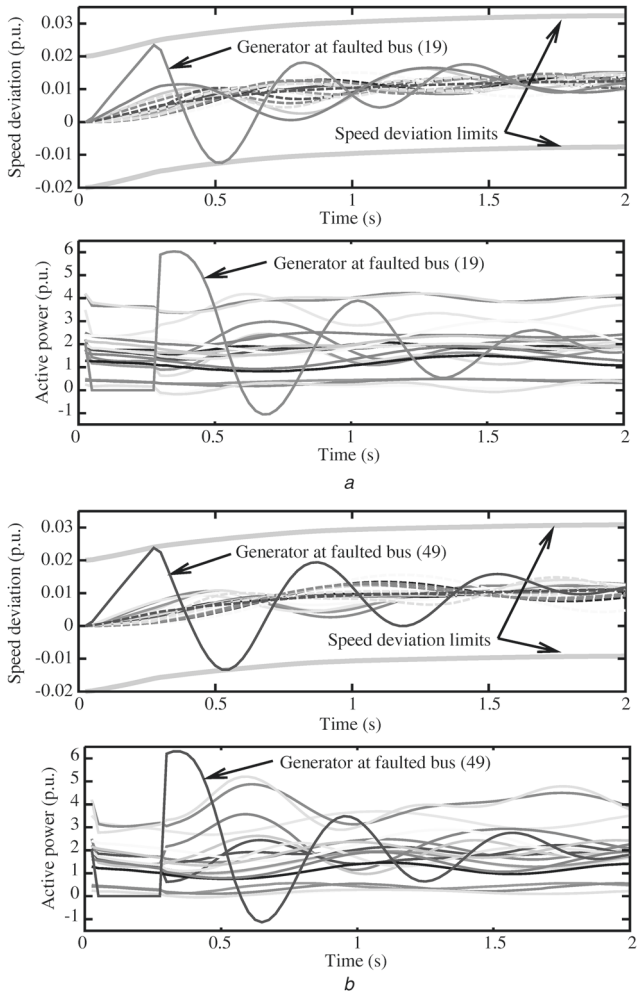

Fig. 8 *Speed deviations in the IEEE 118 bus system as provided by the MC TSCOPF*

a Fault applied at bus 19
b Fault applied at bus 49

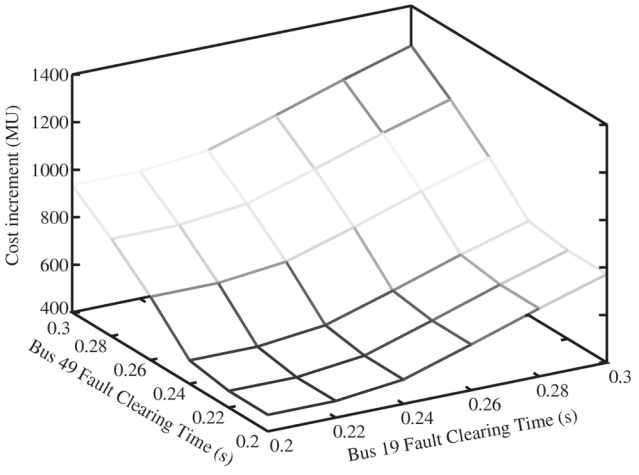

Fig. 9 *Effect of the FCT on the IEEE 118 bus system*

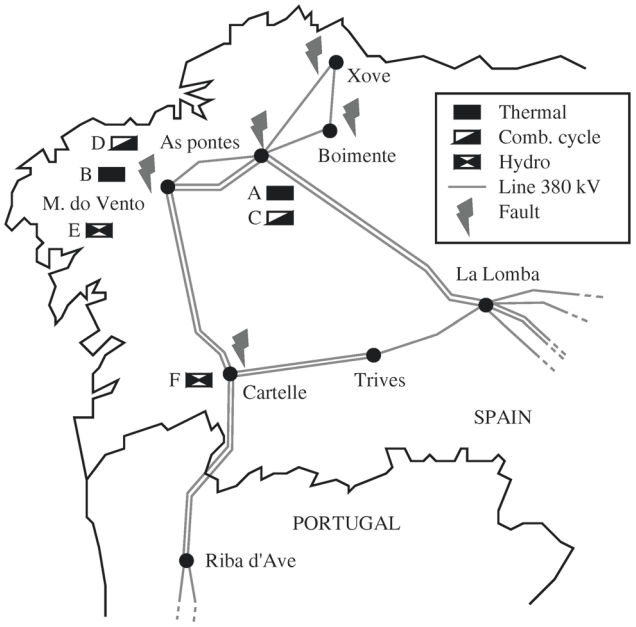

Fig. 10 *MC analysis of the Spanish northwest system*

The proposed method is applied to the economic dispatch provided by the daily market during the peak hour, shown in Column 2 in Table 5. Dynamic simulations using detailed models in PSSE show that the operation point provided by the market results in a loss of rotor angle stability after a fault either at As Pontes or at Meson do Vento substation. The MC TSCOPF is applied taking into account five faults at the substations marked in Fig. 10, using time step $\Delta t = 0.01$ s. An objective function that penalises the deviation from the results of the market is used to represent redispatching costs. Column 3 in Table 5 shows the optimal dispatch provided by the MC TSCOPF when the maximum FCT at each 380 kV substation is 300 ms, which is currently the case when taking into account primary and backup protection systems. It can be seen that power output is reduced at plants A and C, that are connected close to substation As Pontes, and that production costs increases in 13,666 €. This is the minimum cost at which angle stability can be ensured for all five contingences. In all cases, simulations in PSSE using complete detailed models are run to verify the stability of the solution provided by the optimisation model.

Table 5 Power dispatch in megawatts provided by the market and the MC TSCOPF

Plant	Market	FCT 300 ms	FCT 200 ms at As Pontes	FCT 200 ms at As Pontes and Meson do Vento	FCT 200 ms at all substations
A	1250	866	1250	1209	1210
B	320	320	277	320	320
C	550	386	442	438	443
D	50	366	59	50	50
E	200	58	172	200	200
F	200	173	171	171	200
export	370	–31	171	188	223
ΔCost, €	0	13,666	7115	6286	5922

Table 6 Redispatching costs according with the substation where FCT is reduced (minimum costs are marked in bold)

Substation where FCT is reduced to 200 ms	Redispatch cost (first substation), €	Redispatch cost (second substation after As Pontes), €
1. Cartelle	13,275	7113
2. Meson do Vento	13,256	**6286**
3. As Pontes	**7115**	–
4. Boimente	13,666	7115
5. Xove	13,666	7115

The MC TSCOF is also applied to determine the substation(s) where the reduction of the FCT down to 200 ms results in the highest economic saving. Table 6 shows that substation As Pontes is the most suitable, because it results in a cost reduction from 13,666 down to 7115 € (48%). Column 3 shows that once the protection at As Pontes is made faster, the next investment should be made at Meson do Vento because it reduces redispatching costs down to 6286 €. Columns 4–6 in Table 5 show the power dispatch corresponding to these two cases and to a complete upgrade of all substations to an FCT of 200 ms.

6 Conclusion

An MC TSCOF model that retains the dynamics of all synchronous generators is proposed. To improve the applicability of the model, a method that automatically builds the model in GAMS and solves it using a standard solver is presented. The simulation of the dynamics of all power plants makes it possible to account for complex patterns of oscillations. The evolution of the dynamic variables is observed directly on the solution of the model. The method has been successfully tested on systems with up to 20 synchronous generators. No convergence problems have been observed.

A TS criterion based on the synchronous generators speed deviation is proposed. One example in which this constraint provides better results than the classical criterion based on rotor angle is provided.

The proposed method is applied to the Spanish northwest system in order to evaluate the economic cost of ensuring TS after a variety of disturbances. An economic assessment of the impact of installing faster protections in the 380 kV substations is also performed. Using the proposed method, the substations where reducing the FCT contributes to the largest reduction of redispatch costs are identified.

7 Acknowledgment

The authors acknowledge the Ministry of Science and Technology of Spain (Project RESMART, ENE2013-48690-C2-1-R).

8 References

1 Xu, Y., Dong, Z.Y., Xu, Z., *et al.*: 'Power system transient stability-constrained optimal power flow: a comprehensive review'. 2012 IEEE Power and Energy Society General Meeting, 2012, pp. 1–7
2 Moyano, C.F., Castronuovo, E.: 'Non-linear mathematical programming applied to electric power systems stability', in: 'Optimization advances in electric power systems' (Nova Science Publishers, Inc., 2009)
3 Capitanescu, F., Martinez Ramos, J.L., Panciatici, P., *et al.*: 'State-of-the-art, challenges, and future trends in security constrained optimal power flow', *Electr. Power Syst. Res.*, 2011, **81**, (8), pp. 1731–1741
4 La Scala, M., Trovato, M., Antonelli, C.: 'On-line dynamic preventive control: an algorithm for transient security dispatch', *IEEE Trans. Power Syst.*, 1998, **13**, (2), pp. 601–610
5 De Tuglie, E., La Scala, M., Scarpellini, P.: 'Real-time preventive actions for the enhancement of voltage-degraded trajectories', *IEEE Trans. Power Syst.*, 1999, **14**, (2), pp. 561–568
6 De Tuglie, E., Dicorato, M., La Scala, M., *et al.*: 'A corrective control for angle and voltage stability enhancement on the transient time-scale', *IEEE Trans. Power Syst.*, 2000, **15**, (4), pp. 1345–1353
7 Bruno, S., De Tuglie, E., La Scala, M.: 'Transient security dispatch for the concurrent optimization of plural postulated contingencies', *IEEE Trans. Power Syst.*, 2002, **17**, (3), pp. 707–714
8 Xu, Y., Dong, Z.Y., Meng, K., *et al.*: 'A hybrid method for transient stability-constrained optimal power flow computation', *IEEE Trans. Power Syst.*, 2012, **27**, (4), pp. 1769–1777
9 Xin, H., Gan, D., Huang, Z., *et al.*: 'Applications of stability-constrained optimal power flow in the East China system', *IEEE Trans. Power Syst.*, 2010, **25**, (3), pp. 1423–1433
10 Paramasivam, M., Salloum, A., Ajjarapu, V., *et al.*: 'Dynamic optimization based reactive power planning to mitigate slow voltage recovery and short term voltage instability', *IEEE Trans. Power Syst.*, 2013, **28**, (4), pp. 3865–3873

11 Zarate-Minano, R., Van Cutsem, T., Milano, F., *et al*.: 'Securing transient stability using time-domain simulations within an optimal power flow', *IEEE Trans. Power Syst.*, 2010, **25**, (1), pp. 243–253
12 Ruiz-Vega, D., Pavella, M.: 'A comprehensive approach to transient stability control. I. Near optimal preventive control', *IEEE Trans. Power Syst.*, 2003, **18**, (4), pp. 1446–1453
13 Pizano-Martianez, A., Fuerte-Esquivel, C.R., Ruiz-Vega, D.: 'Global transient stability-constrained optimal power flow using an OMIB reference trajectory', *IEEE Trans. Power Syst.*, 2010, **25**, (1), pp. 392–403
14 Xia, S.W., Zhou, B., Chan, K.W., *et al*.: 'An improved GSO method for discontinuous non-convex transient stability constrained optimal power flow with complex system model', *Int. J. Electr. Power Energy Syst.*, 2015, **64**, pp. 483–492
15 Pizano-Martínez, A., Fuerte-Esquivel, C.R., Zamora-Cárdenas, E., *et al*.: 'Selective transient stability-constrained optimal power flow using a SIME and trajectory sensitivity unified analysis', *Electr. Power Syst. Res.*, 2014, **109**, pp. 32–44
16 Ahmadi, H., Ghasemi, H., Haddadi, A.M. *et al*.: 'Two approaches to transient stability-constrained optimal power flow', *Int. J. Electr. Power Energy Syst.*, 2013, **47**, pp. 181–192
17 'A novel margin sensitivity based method for transient stability constrained optimal power flow'. Available at http://www.sciencedirect.com/science/article/pii/S0378779613002940, accessed: 23 May 2016
18 Chen, L., Taka, Y., Okamoto, H., *et al*.: 'Optimal operation solutions of power systems with transient stability constraints', *IEEE Trans. Circuits Syst. Fundam. Theory Appl.*, 2001, **48**, (3), pp. 327–339
19 Xia, Y., Chan, K.W., Liu, M.: 'Direct nonlinear primal-dual interior-point method for transient stability constrained optimal power flow', *Gener. Transm. Distrib. IEE Proc.*, 2005, **152**, (1), pp. 11–16
20 Sun, Y., Xinlin, Y., Wang, H.F.: 'Approach for optimal power flow with transient stability constraints', *Gener. Transm. Distrib. IEE Proc.*, 2004, **151**, (1), pp. 8–18
21 Gan, D., Thomas, R.J., Zimmerman, R.D.: 'Stability-constrained optimal power flow', *IEEE Trans. Power Syst.*, 2000, **15**, (2), pp. 535–540
22 Layden, D., Jeyasurya, B.: 'Integrating security constraints in optimal power flow studies'. IEEE Power Engineering Society General Meeting, 2004, 2004, vol. 1, pp. 125–129
23 Yuan, Y., Kubokawa, J., Sasaki, H.: 'A solution of optimal power flow with multicontingency transient stability constraints', *IEEE Trans. Power Syst.*, 2003, **18**, (3), pp. 1094–1102
24 Calle, I.A., Ledesma, P., Castronuovo, E.D.: 'Advanced application of transient stability constrained-optimal power flow to a transmission system including an HVDC-LCC link', *IET Gener. Transm. Distrib.*, 2015, **9**, (13), pp. 1765–1772
25 'IEEE guide for synchronous generator modeling practices and applications in power system stability analyses'. IEEE Std. 1110-2002 Revis. IEEE Std. 1110-1991, 2003, p. 0_1-72
26 Jiang, Q., Geng, G.: 'A reduced-space interior point method for transient stability constrained optimal power flow', *IEEE Trans. Power Syst.*, 2010, **25**, (3), pp. 1232–1240
27 Geng, G., Jiang, Q.: 'A two-level parallel decomposition approach for transient stability constrained optimal power flow', *IEEE Trans. Power Syst.*, 2012, **27**, (4), pp. 2063–2073
28 Geng, G., Ajjarapu, V., Jiang, Q.: 'A hybrid dynamic optimization approach for stability constrained optimal power flow', *IEEE Trans. Power Syst.*, 2014, **29**, (5), pp. 2138–2149
29 Jiang, Q., Zhou, B., Zhang, M.: 'Parallel augment Lagrangian relaxation method for transient stability constrained unit commitment', *IEEE Trans. Power Syst.*, 2013, **28**, (2), pp. 1140–1148
30 Xu, Y., Dong, Z.Y., Zhang, R., *et al*.: 'A decomposition-based practical approach to transient stability-constrained unit commitment', *IEEE Trans. Power Syst.*, 2015, **30**, (3), pp. 1455–1464
31 'GAMS Home Page'. Available at https://www.gams.com/, accessed: 05 June 2016
32 Grainger, J.J., Stevenson, W.D. Jr.: 'Power system analysis' (McGraw-Hill Science/Engineering/Math, New York, 1994, 1st edn.)
33 Zhu, J.: 'Optimization of power system operation' (John Wiley & Sons, 2009)
34 Kundur, P.: 'Power system stability and control' (McGraw-Hill Professional, 1994)
35 Anderson, P.M., Fouad, A.A.: 'Power system control and stability' (Wiley-IEEE Press, 2002, 2nd edn.)
36 Siemens TI, Ed.: 'BOSL controllers – standard 1'. 2008
37 'IPOPT' Availableat https://www.projects.coin-or.org/Ipopt, accessed: 23 May 2016
38 Wächter, A.: 'An interior point algorithm for large-scale nonlinear optimization with applications in process engineering', PhD thesis, Carnegie Mellon University, Pittsburgh, PA, 2002
39 'IEEE 118 bus test case data'. Available at http://www.motor.ece.iit.edu/data/JEAS_IEEE118.doc, accessed: 23 May 2016
40 'Power flow cases – Illinois Center for a Smarter Electric Grid (ICSEG)'.
41 'TEST SYSTEM REPORT development of a comprehensive power system simulation laboratory'. Available at http://www.itee.uq.edu.au/pssl/drupal7_with_innTheme/?q=node/374, accessed: 23 May 2016
42 UCTE Union for the Coordination of Transmission of Energy: 'Final Report – System Disturbance on 4 November 2006'. 2007

9 Appendix

See Tables 7 and 8.

The Python program that builds the model in GAMS, the GAMS model and the IEEE 118 bus system data in PSSE raw format are published online in http://www.e-archivo.uc3m.es/handle/10016/23105.

Table 8 IEEE 118 bus system generator cost data

Gen.	Max P, MW	a	b	c	Gen.	Max P, MW	a	b	c
10	300	7	13	11	66	420	64	83	11
12	300	7	13	11	69	300	7	13	11
19	300	33	11	5	76	100	10	18	13
25	300	7	13	11	80	300	7	13	11
26	350	33	11	3	87	300	33	11	3
32	100	10	18	13	89	200	7	13	11
49	300	28	10	6	92	300	7	13	11
54	250	28	12	3	100	300	7	13	11
61	200	39	13	4	111	100	10	18	13
65	420	64	83	11	113	100	10	18	13

Here, a is in M.U.; b is in M.U./MW; and c is in 10^{-3} M.U./MW^2

Table 7 Dynamic parameters of generators and controllers in the IEEE 118 bus system

H	D	r_a	x_d	x'_d	x_q	x'_q	T'_{d0}	T'_{q0}	K_{EXC}	T_{EXC}	K_{TG}	T_{TG}
3	2	0	1.5	0.3	1.5	0.3	6	0.5	100	1.0	50	1.0

Data in per unit referred to the generator nominal power